NASA CONTRACTOR REPORT

NASA CR-1894

Corrected Copy

EXPERIMENTAL DETERMINATION OF PRESSURE DROP AND FLOW CHARACTERISTICS OF DILUTE GAS-SOLID SUSPENSIONS

by Robert Pfeffer and Salvatore J. Rossetti

Prepared by
CITY COLLEGE OF THE CITY UNIVERSITY OF NEW YORK
New York, N.Y. 10031
for Lewis Research Center

NATIONAL AERONAUTICS AND SPACE ADMINISTRATION • WASHINGTON, D. C. • AUGUST 1971

1. Report No. NASA CR-1894	2. Government Accession No.	3. Recipient's Catalog No.
4. Title and Subtitle EXPERIMENTAL DETERMINATION OF PRESSURE DROP AND FLOW CHARACTERISTICS OF DILUTE GAS-SOLID SUSPENSIONS		5. Report Date August 1971 6. Performing Organization Code
7. Author(s) Robert Pfeffer and Salvatore J. Rossetti		8. Performing Organization Report No. None 10. Work Unit No.
9. Performing Organization Name and Address City College of the City University of New York Convent Avenue at 138th Street New York, New York 10031		11. Contract or Grant No. NGL-33-013-029 13. Type of Report and Period Covered Contractor Report
12. Sponsoring Agency Name and Address National Aeronautics and Space Administration Washington, D.C. 20546		14. Sponsoring Agency Code
15. Supplementary Notes		

16. Abstract

The effect of solids loading ratio, particle size, and gas Reynolds numbers on the pressure drop and flow characteristics of a dilute gas-solid suspension in turbulent pipe flow has been studied experimentally. Glass beads of 10 to 60 micron diameter were used with air Reynolds numbers of 10,000 to 25,000 and solids loading ratios of up to 2.5. Drag reduction has been found to occur for certain particle sizes in both vertical and horizontal flow. An explanation based on the interaction of the particles with the turbulent structure of the fluid near the wall has been suggested.

17. Key Words (Suggested by Author(s)) Particles Pipe flow Pressure drop Drag reduction Suspension Dilute Loading ratio Air	18. Distribution Statement Unclassified - unlimited		
19. Security Classif. (of this report) Unclassified	20. Security Classif. (of this page) Unclassified	21. No. of Pages 49	22. Price* $3.00

*For sale by the National Technical Information Service, Springfield, Virginia 22151

FOREWORD

The research described in this report was conducted by the City College of the City University of New York under NASA grant NGL-33-013-029. Mr. Henry A. Putre of the Lewis Research Center Nuclear Systems Division was the NASA Project Manager.

Table of Contents

Table of Contents (cont.)

Summary

A closed loop experimental apparatus was assembled for the purpose of making pressure drop and turbulence measurements for dilute gas-solid suspensions flowing in a tube. The apparatus included a two phase flow meter for solids concentration determination and solid state anemometry for velocity and turbulence measurements.

Five different sizes of glass beads ranging from a nominal diameter of 10 to 60 microns were circulated at loading ratios up to 2.5. Three different gas Reynolds number ranges from 12,000 to 25,000 were investigated in both a vertical and horizontal test section.

The results of the investigation showed that in the vertical test section lower pressure drops were obtained for all of the dilute gas-solid suspensions studied than were observed for tne pure gas at the same gas Reynolds number. For the horizontal test section pressure drop increases above the pure gas values were found for the two largest cited particles but decreases were also observed with the smaller particles.

The vertical test section results may be explained in terms of the interaction of the particles with the turbulent structure of the fluid in the vicinity of the wall. The particle relaxation time was an important factor and a particle size of 30 microns was found to yield the greatest reduction in frictional pressure loss. Both smaller and larger particles resulted in less drag reduction. The results of the horizontal test section could not be wholly explained on this basis due to the "segregated" and "bouncing" flow phenomena observed with the larger particles.

Turbulence measurements made in a vertical section show an increase in the centerline intensity of turbulence when drag reduction was observed. These preliminary measurements might indicate that a build-up of the laminar sublayer is caused by the particles extracting angular momentum from the fluid near the wall. Similar trends have been reported in cases of drag reduction with liquids.

Introduction

Historically, the first use of gas-solid suspensions occurred in the conveying of food and materials. When the unique contacting properties of suspensions of finely divided materials in a gas became evident, however, their application was no longer limited to conveying materials, but spread to include many physical and chemical operations as well. Gas-solid suspensions are now being considered as nuclear reactor coolants and as working fluids in conventional gas power cycles for space power generation.

Even though gas-solid suspensions find such widespread applications, the prediction of pressure losses associated with their flow is still mostly an empirical art. One would expect that as the suspensions become less and less concentrated the flow properties would be more readily characterized and more easily understood, since they approach those of the gas. However, the opposite is true. The flow of dilute gas-solid suspensions is even less predictable than that of concentrated suspensions.

Many analytical approaches attempting to describe the flow characteristics of gas-solid suspensions appear in the literature. Soo and coworkers have studied many different aspects of gas-solid flow and their work is very valuable in obtaining an insight into some of the complex effects of the interactions of the particles with the flowing gas. A summary of Soo's work as well as many other important contributions to the theory of gas-solid suspension flow can be found in Soo's recent text "Fluid Dynamics of Multiphase Systems" (ref. 1).

Saffman (ref.2) presented the equations of motion of a gas carrying small dust particles and derived the equations satisfied by small disturbances in a steady laminar flow. His analysis indicated that under certain conditions fine dust had a stabilizing

action and that the pressure drop of a suspension could be less than that of a pure gas. Julian and Dukler (ref. 3) presented correlations for the pressure drop caused by a flowing gas-solid suspension computed by use of an eddy viscosity model. These correlations indicated that the pressure drop of a suspension should monotonically increase as particle concentration increases. Pfeffer, Rossetti and Lieblein (ref. 4) applied the Reynolds analogy between heat and momentum transfer to obtain a correlation for the pressure drop associated with flowing suspensions. Boothroyd (ref. 5) used dimensional analysis in an attempt to understand the flow of suspensions. However, due to the inherent assumptions necessary with each of the analytical approaches and seemingly conflicting or inadequate experimental results none of the analyses has proven to be completely adequate.

Experimental investigations using large particles (particle diameter > 100 microns((refs. 6-11) have found that the addition of solid particles to a turbulently flowing gas will always increase the frictional resistance to flow. Studies using small particles (refs. 12-17) have also reported this drag increase. Other investigators using small particles have, however, reported a decrease in the frictional resistance below that of the pure gas at low solids loading ratios (refs. 5, 18, and 19). This phenomenon commonly referred to as "drag reduction" has been found to occur upon the addition of small amounts of viscoelastic material to liquids (refs. 20-23) and also in the flow of liquid-solid suspensions (refs. 24 and 25). However, drag reduction with gas-solid suspensions is a dubious phenomenon with meager evidence supporting it.

The objectives of this study were to determine the effects of certain significant variables such as particle concentration

(loading ratio), particle diameter and gas Reynolds number on the pressure drop and flow characteristics of a suspension flowing through a tube in fully developed turbulent flow. Particular attention was given to suspensions having a loading ratio of solids to gas flow rates of less than one so as to investigate the extent of drag reduction. In addition, the effect of horizontal or vertical transport of these suspensions was also investigated.

Experimental Apparatus and Materials

The apparatus employed in this study was based on the use of a circulating compressor capable of pumping both gas and solids together without damage to its internal parts or causing any contamination of the suspension. This compressor thus permitted design of a closed (recirculating) experimental loop. Pressure drop across both horizontal and vertical test sections were measured by means of micromanometers. Velocity and turbulence measurements were made with an anemometer equipped with a quartz coated thermister probe capable of withstanding the impacts of the solid particles. Particle concentration was determined with a specially designed two phase mass flow meter employing strain gages. In order to properly calibrate the mass flow meter, the closed loop was modified for open-loop operation. Five different sizes of glass beads were used in the experiments in order to determine the effect of particle diameter on frictional pressure loss. Some of the details concerning the apparatus and materials employed in the study are presented below; additional information can be obtained from reference 26.

A schematic diagram of the experimental loop is shown in figure 1. The loop was primarily constructed of 1" O.D. stainless steel tubing but also contained four pyrex glass viewing sections.

Flow is in the counterclockwise direction and is accomplished by the gas-solids circulator. This circulator was designed and built by the Franklin Institute and donated to the City College for this research by the Bureau of Mines at Morgantown, West Virginia. The circulator was driven by a 15 horsepower variable speed induction motor powered by a 25 horsepower motor coupled with a variable frequency generator. The motor generator provided stepless speed variations in two ranges from 1600 to 6000 and from 2640 to 13200 rpm.

In order to promote uniform particle distribution sharp 90^{o} elbows were installed before every section of the loop where measurements were taken. The vertical test section was 30" long and was located approximately 5 feet from the elbow in the upward vertical leg of the loop. The horizontal test section was 40" long and was preceded by a calming section of approximately 8 feet in length. The downward vertical leg of the loop contained an orifice plate, the two phase flow meter and the anemometer probe inlet. A particle inlet port used in open loop operation follows the anemometer probe inlet.

A cross section of the two phase mass flow meter, designed by the Bureau of Mines is shown in figure 2. The metering element is a target attached to a rod at the end of a cantilevered metal strip to which are affixed metal foil strain gages. The strain gages sense the deflections of the flexible metal strip caused by the solid and gas acting on the target. The deflection is monitored continuously by a recorder which also continuously monitored the temperature in the loop.

The anemometer probe used in this study was a thermistor probe developed by the DISA S&B Corp. This probe was L shaped and had a glass coated thermistor bead suspended at the tip.

The L-shape of the probe allowed velocity measurements to be taken without interference from the support rod. The thick glass coating prevented the particles from damaging the thermistor or interfering with the measurement. One such probe was tested in the closed loop for ½ hour of continuous operation under conditions of heavy particle loading using large diameter particles. At the end of this time it was found that the probe had not changed calibration.

The lower horizontal leg of the loop contains a pitot static tube assembly which was used for calibrating the anemometer probe and a particle inlet which was used to fill the loop during closed loop operation. At the end of the bottom horizontal section of the loop there is a three way ball valve which was used to clean the loop through a sintered metal filter.

Closed loop experiments were run with suspensions containing particles of five different particle sizes. These experiments were performed by adding small amounts of particles, usually in 5 or 10 gram increments to the loop through the opening downstream of the pitot static section and then circulating the particles, taking strain gage, anemometer, orifice and vertical and horizontal pressure drop readings. The nominal particle sizes of the five different size glass beads studied are shown in Table I.

TABLE I. - PARTICLE SIZES

Descriptive Title	Actual Nominal Particle size*
50μ	59μ
30μ	34μ
#279	25μ
#981	20μ
#980	10μ

*Determined by Coulter Counter Analysis

Size distribution analyses were made both photographically and by use of a Coulter counter. Figure 3 shows microphotographs of the 30μ glass beads both before and after circulation through the loop. As can be seen from the figure the particles are spherical in shape and fairly uniform in size both before and after circulation through the loop.

Calibration Procedure and Data Analysis

In order to obtain meaningful results with the two phase flow meter it first had to be calibrated in an open loop system under various conditions of solids loading and gas flow rate.

A schematic diagram of the open loop system used for calibration of the flow meter is shown in figure 4. Particles were fed in by using a helix type volumetric dry feeder into a rotary air lock. The air lock permitted continuous feeding without allowing additional air to be introduced in the system. A vibrator was installed on the inlet Y to maintain continuous flow into the loop. The air velocity was measured by a pitot static tube assembly placed upstream of the particle entrance.

The collector was essentially a cyclone with sintered tubes providing the air outlet. This design prevented solids contamination of the air and also prevented extensive clogging of the sintered tubes. The two phase flow meter was calibrated by weighing the particles collected per unit time during open loop operation. The data obtained were correlated by applying a simple mementum balance.

The strain gage reading obtained from the two-phase flow meter is proportional to the force which the fluid exerts on the circular target inserted in the stream. This force is equal to the time rate of change of momentum of the suspension, so that

$$V_{ST} \propto F = \frac{d(m_s v_s)}{dt} \tag{1}$$

The suspension is composed of both gas and solids, therefore, equation (1) can be written as

$$V_{ST} = K_1 \frac{d(m_g v_g)}{dt} + K_2 \frac{d(m_p v_p)}{dt} \tag{2}$$

Expansion of this equation with the assumption that there is no slip between the particle and gas and that there is no acceleration yields

$$V_{ST} = K_1 v_g \left(\frac{dm_g}{dt} + \frac{K_2}{K_1} \frac{dm_p}{dt} \right) \tag{3}$$

however,

$$\frac{dm_g}{dt} = \rho_g v_g A \tag{4}$$

and

$$\frac{dm_p}{dt} = W_P \tag{5}$$

so that equation (3) can be written as

$$V_{ST} = K_1' \rho_g v_g (\rho_g v_g) + K_2' \rho_g v_g (W_P) \tag{6}$$

Since the area of the target does not occupy the entire flow area of the tube, it is entirely possible that the relations between V_{ST} and the mass flow rate of gas and solids is not linear so that an equation of the form,

$$V_{ST} = K_1'(\rho_g v_g)(\rho_g v_g)^a + K_2'(\rho_g v_g)(W_P)^b \qquad (7)$$

may be expected. The experimental data were found to fit equation (7) very well and "best values" of the constants were determined to give

$$V_{ST} = 0.0128(\rho_g v_c)(\rho_g v_c)^{0.808} + 0.0155(\rho_g v_c)(W_P)^{0.808} \qquad (8)$$

where v_c the centerline gas velocity has been used to replace v_g the average gas velocity for convenience purposes. It is interesting to note that the constants a and b were both found to have the same value. Since the loading ratio, η, is defined as the ratio of the particle flow rate, W_p, and the gas mass flow rate, $0.8\ \rho_g v_c A$, the final correlation can be expressed in terms of η as

$$\eta = \left[\frac{V_{ST}}{0.0217(\rho_g v_c)^{1.808}} - 0.590\right]^{1.238} \qquad (9)$$

Although technically valid only for the 30μ particles which were used in the calibration runs, this correlation was used to determine loading ratios for all the glass particles studied in this work.

After calibration of the two phase flow meter, attention was turned to running the closed loop experiments. In order to make sure that fully developed flow was obtained in both horizontal and vertical test sections, velocity profiles and pressure drops were taken using air as the flowing fluid. The thermistor anemometer probe which was used to determine gas velocity profiles

during closed loop operation with suspensions was also calibrated against the pitot tube in the lower horizontal section, as was the orifice upstream of the two phase flow meter.

Velocity profiles were obtained for tube Reynolds numbers from 10,000 to 40,000. A typical set of data is shown in figure 5. The figure shows a plot of the curve obtained by using the 1/7th power law based on the experimentally determined centerline velocity. The greeement between the data and the predicted curves was better than 3%.

Figure 6 shows the experimentally measured friction factor versus Reynolds number curves for the horizontal test section. The data are compared with the recommended correlation (ref. 27)

$$f = 0.184\ Re^{-0.2} \tag{10}$$

and are seen to be within $\pm$5%. The vertical test section data seemed to fit the other recommended correlation (ref. 27)

$$f = 0.0056 + 0.5\ Re^{-0.32} \tag{11}$$

slightly better and are compared with this correlation in figure 7. Again the agreement is within $\pm$5% of the correlation.

Having completed the calibration and pure gas runs, data were collected for suspensions flowing in the closed loop. Friction factors for both suspension flow and pure gas flow were calculated using the common relation for incompressible gas flow

$$f = \frac{2g_c\ \Delta PD}{\rho_g \bar{v}^2 L} \tag{12}$$

where the friction factor is calculated by using the gas density and an average gas velocity ($\bar{v} = 0.8\ v_c$) for each case. Since the pressure drop is very small compared to the static pressure and because the loop flow is essentially isothermal, acceleration effects are negligible and

$$\Delta P = \Delta P_m \tag{13a}$$

for the horizontal test section and

$$\Delta P = \Delta P_m - \eta \rho_g L \tag{13b}$$

for the vertical test section where ΔP_m is the measured pressure drop. The friction factors calculated by these relations for the suspension were then divided by friction factors calculated by equation (10) for horizontal test section data and equation (11) for vertical test section data at the same gas Reynolds number. The friction factor ratio for the horizontal section therefore represents the ratio of suspension to air pressure drop at a given Reynolds number. For the vertical test section this friction factor ratio is the pressure drop ratio corrected for the solids head in the section.

Experimental Results

During closed-loop experimental operations with a suspension as the working fluid, mass flow ratios, friction factors for both vertical and horizontal test sections, centerline velocity and percent turbulence as well as orifice coefficients were determined. In addition, a photographic analysis using the pyrex section preceding the horizontal test section was performed for representative Reynolds number and loading ratio conditions. Particle size

distribution analyses were also made on representative particulate samples both before and after circulation through the loop. The results of these analyses and experiments are presented and discussed below.

Curves of loading ratio as a function of weight of particles added to the system were obtained for the five particle sizes at each of three different Reynolds number ranges. These are shown in Figure 8 for the 30μ particles and are typical of the type of results obtained with all but the smallest particles. With the exception of these #980 glass beads (average D_p = 10μ) all of the curves were roughly S-shaped. For each particle size a comparison of the plots for the three different Reynolds numbers indicated that the higher the Reynolds number the higher the loading ratio at any given weight added to the system. The effect was more pronounced as the weight added to the loop increased. This can be explained by the fact that a larger percentage of particles are entrained by the gas when its velocity is high as compared to when it is low. At low air velocities it is more likely that particles will be trapped in the compressor, elbows or other sections of the loop. It should also be pointed out that particles will remain in suspension at higher concentrations for higher air velocities.

The shape of these curves can be explained on the basis of differing interacting effects. The lower portion of the curves is less steep and indicates that a small percentage of the particles added to the system are actually circulating. For the larger particles this effect was more pronounced than for smaller particles and is primarily due to the particles accumulating in irregularities in the loop. For the smaller particles the effect can also be attributed to their cohesiveness which initially makes them more difficult to circulate and possibly indicates a tendency

for those particles to coat the surface of the loop (although this was not visually observed except for the smallest size glass beads). The steep portion of the curves appears to occur after the surface irregularities are filled and after cohesive forces are no longer sufficient to prevent additional particles from being circulated.

After this steep portion, the figure indicates a second flattened part of the curves. In this region adding more particles to the system does not appear to significantly increase the amount of circulating material. This is a result of particle sedimentation, so that as particles are added other particles settle out at approximately the same rate. This sedimentation can be partially attributed to the size of the particles, as the 50μ particles exhibit this second flattened portion of the curve at the lowest concentration for the highest Reynolds number studies. However, since this flattening out occurs at approximately the same loading ratio (at the same Reynolds number) for the other particles and since at the lower Reynolds numbers the smaller particles exhibited flat portions at the same or lower concentration than the large particles, a more complicated explanation is indicated. The cohesiveness of the fine particles almost certainly will tend to cause sedimentation at lower concentration than would be otherwise expected. Furthermore, the lower the velocity the more important the cohesive force since re-entrainment in the fluid stream becomes more difficult.

The smallest particles (#980 glass beads) did not exhibit the previously discussed S shaped curves. The curves obtained for these particles were extremely flat, indicating difficulty of entrainment. Furthermore, it was also found that with these particles humidity strongly affected the loading ratio obtained

at a given weight added to the system. At high humidity few particles could be circulated at any but the highest Reynolds number. These results tend to confirm that particle cohesiveness plays an important role in determining loading ratio characteristics.

By measuring the pressure drop across the orifice and assuming an average velocity of 0.8 times the centerline velocity measured by the anamometer, orifice coefficients were also calculated for all of the closed loop runs at different particle loading ratios and Reynolds numbers. These results are plotted in figure 9 along with a curve representing the orifice calibration obtained with pure air as the circulating fluid. Dashed curves representing a $\pm 5\%$ deviation from this curve are also shown. Since very few data points fall outside of these dashed curves it appears that the orifice coefficient was not affected by the presence of particles in the flow stream. These results confirm Orr's contention (ref. 28) that a properly calibrated orifice can be used to determine gas mass flow rates for dilute suspensions.

The pressure drop data obtained were analyzed by plotting the ratio of the friction factor with and without particles at the same gas Reynolds number as a function of solids loading ratio for both the horizontal and vertical test sections for each of the five particle sizes and each of three Reynolds number ranges studied. A great deal of data were taken and although the points showed quite a bit of scatter (all of the data points can be found in ref. 26), curves were faired in by eye to represent the data.

Figure 10 shows the curves thus obtained for the 50μ particles. The figure shows an increase in the friction factor

ratio as the loading ratio increased for each Reynolds number in the horizontal test section. The largest increase occurred at the lowest Reynolds number. In the vertical test section the curves show a large decrease in friction factor as loading ratio is increased. The "drag reduction" is found to be greatest at the highest Reynolds number. In other words, the lower the Reynolds number, the higher the friction factor ratio for both the vertical and horizontal sections. The figure also indicates that at the higher Reynolds number the friction factor ratio appears to have an inflection perhaps indicating a tendency to reach a minimum.

The results obtained using the 30μ particles appear to exhibit similar trends as shown by figure 11. The figure indicates less drag increase in the horizontal test section and slightly greater drag reduction in the vertical section at the highest Reynolds number considered.

The results obtained using the #279 glass beads shown in figure 12 indicate that with these particles drag reduction is also found in the horizontal section at the two highest Reynolds numbers. However, the decrease is at most 18% and there is a slight drag increase at the lowest Reynolds number condition. The results in the vertical test section again indicate drag reduction, but not to the same extent as with the larger particles. No inflection was observed for the vertical test section results up to the highest loading ratio investigated.

The #981 glass beads were very similar to the #279 beads - having a mean diameter of 20μ compared to 25μ for the #279 beads. However, the #981 beads had a somewhat different size distribution. In view of their size similarity, it was not surprising that the results for the #981 glass beads in both the horizontal and vertical

test sections as shown in figure 13 exhibited the same general trends and magnitudes as those for the #279 glass beads. The only exception to this agreement appears in the horizontal data at the lowest Reynolds number where a slight drag reduction rather than a slight drag increase is shown. This could be attributed to the fact that the #279 glass beads contained more larger particles than the #981 glass beads. This is also the probable reason that all of the horizontal test section friction factor results are slightly lower than for the #279 glass beads.

The smallest particles used in this investigation were the #980 glass beads (average D_p=10μ). The results with these particles showed practically no effect of Reynolds number. As seen in figure 14 these particles gave slight drag reduction in both horizontal and vertical test sections. Furthermore, there appears to be very little difference in the results for both test sections.

In order to show more clearly the effect of particle size on the friction factor ratio, two sets of additional curves were prepared. These are shown in figures 15 and 16. Figure 15 shows the results of friction factor ratio as a function of loading ratio for the five different particle sizes at the highest Reynolds number in the horizontal section. The figure clearly shows that the 50μ and 30μ particles result in drag increases, whereas, the #279, #981 and #980 glass beads cause drag reduction of approximately the same order of magnitude, but less than that exhibited for the same particles in the vertical section.

The vertical section results shown in figure 16 indicate that the maximum drag reduction is obtained for the 30μ particles with the 50μ particles giving only slightly more drag. The #981 and #279 glass beads gave approximately the same magnitude of drag

reduction - a value less than achieved with the larger particles. The smallest particles appear to give the least drag reduction.

Discussion of Results

The best explanation for the vertical test section results appears to be given by a theoretical analysis on the stability of a dusty gas by Saffman (ref. 2). In this analysis, Saffman showed that if the particles are fine enough for the relaxation time, which is a measure of the rate at which the velocity of a particle adjusts to changes in the gas velocity, to be small compared with the time scale of the turbulent eddies, then the addition of particles causes the critical Reynolds number for transition from laminar to turbulent flow to be decreased and a drag increase results which is proportional to the increased density of the fluid. However, he predicts that if the particles are coarse so that the relaxation time is relatively large, then the suspension has a stabilizing action (the particles cause a higher critical Reynolds number and less frictional pressure loss). In other words, the finite slip velocity between the particles and the gas causes energy to be extracted from the turbulent eddies resulting in a smaller frictional dissipation at the wall. As indicated by the work of Soo, (ref. 1) this energy extraction would be especially pronounced in the vicinity of the wall where the velocity of the particles greatly exceeds that of the gas.

From Saffman's analysis it would be expected that the larger particles which lag behind the turbulent fluctuations of the flowing air, will yield more drag reduction than smaller particles, which to some extent follow the turbulent fluctuations of the fluid. The fact that the 50μ particles yield slightly less drag reduction than the 30μ particles in the vertical test section is also reasonable, since according to this model, increasing the size of

particles already having a relaxation time very much greater than the characteristic time scale of the eddies lessens the stabilizing effect at a given particle concentration. At the gas Reynolds numbers studied in this investigation it would appear that the 30μ particles yield the optimum relaxation time since both larger and smaller sized particles result in less drag reduction.

The results for the horizontal test section cannot be fully explained on the basis of the theory just presented. The reason for this is apparently due to gravitational effects which cause the particle number density to vary across the tube and not remain constant as required by Saffman's analysis. Because of gravity the larger particles tend to congregate in the lower half of the horizontal section. As the particles become smaller, their sedimentation velocity decreases, hence decreasing the tendency toward "segregated flow" resulting in the friction factor ratios for the two sections to approach one another. The fact that the smallest particles used in this study yielded essentially the same results in the horizontal and vertical test sections seems to confirm this theory. With the larger (50μ and 30μ) particles a drag increase was observed in horizontal flow which may be attributed to the fact that many of these particles were transported through the horizontal sections in "bouncing flow" that is, by bouncing along the bottom of the tube. This "bouncing flow" caused additional frictional pressure drop. Since the number density of the particles is not uniform the upper portion of the horizontal section is less affected by the particulate flow, so that the net result is a drag increase for these larger particles. As the particles become smaller the "segregated flow" is minimized and drag reduction results.

These concepts can perhaps be best illustrated by a numerical example. The relaxation time of the particles is calculated as the ratio of the momentum of the particle to the force exerted on it. Assuming that the particles are spheres of diameter D_p and using Stokes drag formula:

$$t_R = \frac{1}{18} D_P^2 \rho_P / \mu \qquad (14)$$

The characteristic time for energy containing eddies may be expressed as (ref. 29)

$$t_e = 0.1\ D/2u_\tau \qquad (15)$$

where u_τ is the conventional friction velocity and the characteristic time for large eddies is

$$t_l = D/2u_\tau \qquad (16)$$

The effect of gravity will make itself felt when the terminal settling velocity of the particle is of the same order of magnitude as the friction velocity; again the terminal settling velocity may be determined by using the Stokes' Law expression.

Table II lists the calculated relaxation time and terminal velocity of the five different size particles. This table will be used in conjunction with calculations made using a typical set of experimental data as indicated below,

Data: $\bar{v}$ = 44.5 ft/sec, $(Re)_g$ = 24,650

ΔP = 1.737 lb/ft^2; D = .0833 ft.

ρ_g = .0790 lb/ft^2; L = 2.5 ft

Calculated Results; U_τ = 2.43 ft./sec

t_e = .0017 sec.

t_l = .017 sec

TABLE II. - PARTICLE RELAXATION TIME AND TERMINAL VELOCITY

PARTICLE SIZE	RELAXATION TIME	TERMINAL VELOCITY
#980 (10μ)	.0026 sec	0.084 ft/sec
#981 (20μ)	.010 sec	0.332 ft/sec
#279 (25μ)	.015 sec	0.483 ft/sec
30μ (34μ)	.031 sec	1.01 ft/sec
50μ (59μ)	.094 sec	3.02 ft/sec

Referring to the calculated relaxation times for the various sized particles in Table II, one would expect, on the basis of Saffman's theory, that drag reduction would occur in the vertical section for this Reynolds number condition for each of the particles since the relaxation times are all greater than t_e. However, it would also be expected that the magnitude of this drag reduction would be smallest for the #980 glass beads where t_R is only slightly greater than t_e. It would also be expected that the maximum drag reduction would occur for particles sized somewhere between the #279 and 30μ particles and decrease for larger sized particles where $t_R > t_l$. These observations are in good agreement with the experimental results for the vertical test section. Results for the horizontal section are complicated by the effect of gravity. The third column of Table II indicates

that the effect of gravity will become prominent for the 30 and 50μ particles where the terminal and friction velocities are of the same order of magnitude. This again is in agreement with the observed results.

Photographs showing the gross flow patterns of the particles under varying conditions of loading and Reynolds number appear to confirm the fact that the smaller particles respond to the turbulent fluctuations of the fluid to a greater extent than the larger particles. Figure 17 shows the gross glow patterns for the #980 glass beads and the 30μ glass beads at two different loading conditions. Here the light areas represent particles. For the small particles it can be seen by the wispiness of this particulate flow that many of the particles are responding to the turbulent fluctuations of the fluid. The photographs of the 30μ glass beads indicate very few of these wisps and also clearly show the segregated flow exhibited in the horizontal section for these particles.

In an effort to clarify some aspects of the drag reduction experimentally, preliminary measurements of the intensity of turbulence were taken at the center of the vertical test section using the thermistor anemometer probe. Figure 18 shows variation of intensity of turbulence ratio with and without particles as a function of loading ratio for each of the five particles studied. These results are somewhat paradoxical in that the ratio of the intensity of turbulence with particles to that of particle free air was found to increase as the particles were added, with the largest increase shown by the 30μ particles which also gave the largest drag reduction. On the basis of the theory presented above, it was expected that these particles would show the largest decrease in the intensity of turbulence. However, it may be that

the interaction of the particles with the turbulence eddies occurs very close to the wall and, that, at the center, the intensity of turbulence is actually greater. Similar results have been found with drag reducing liquids (ref. 30) but it is obvious that many more turbulent intensity measurements must be taken before any reasonable conclusion can be made from these measurements.

Conclusions

A closed-loop system capable of continuously recirculating gas-solid suspensions has been built. This system was used to measure pressure drops, gas velocities, turbulence intensities and particle concentrations with the aid of a solid state anemometry unit and a specially designed and calibrated two-phase mass flow meter. Five different sizes of glass beads were studied during the investigation at three different gas Reynolds number ranges for both a vertical and horizontal test section. From the results of this investigation the following conclusions can be reached:

1. "Drag reduction" does occur with gas-solid suspensions in both horizontal and vertical test sections.
2. The results from the horizontal section in the loading ratio range up to 2.5 indicate that the "drag reduction" is greatest for the smallest particles (approximately 20%). Drag increases of as much as 40% were noted when the two largest size particles were circulated.
3. The vertical test section results for the same loading ratios indicate that "drag reduction" is at an optimum for the 30μ particles (approximately 75%) and that the amount of drag reduction decreases with the larger or smaller particles.

4. Except for the smallest particle size, the friction factor results for the vertical section were always lower than the horizontal section. For the smallest particles the magnitude of the friction factor ratios in both sections was essentially the same.
5. The friction factor results for the vertical section may be explained by an analytical model which assumes energy extraction from the fluid stream rather than energy dissipation at the wall. The energy extracted in the fluid stream can be related to the relaxation time of the particles.
6. At any suspension concentration, the results from both test sections indicate that the lower the Reynolds number the higher the ratio of suspension to gas friction factor. This Reynolds number trend has been reported in many previous experimental investigations even with large particles.
7. Results from the centerline turbulence intensity ratio measurements for the five particle sizes investigated indicate that the per cent turbulence at the center of the tube increases as particles are added to the system. Thus, there appears to be a correlation between the intensity of turbulence at the center of the tube and the amount of drag reduction observed in the vertical test section.

Concluding Remarks

This experimental investigation has shown some remarkable effects of the influence of small particle loadings and different particle size on the pressure drop and flow characteristics associated with turbulent gas-particle flow in a tube. The

phenomenon of drag reduction has been found to occur under certain flow conditions in both vertical and horizontal test sections. At a loading ratio of 1.5 and a gas Reynolds number of 25,000 for example, the friction factor ratio in the vertical test section was found to be as low as 0.27 when transporting 30μ particles in air. This indicates a reduction in drag of close to 75%! An explanation of these results based on the interaction of the particles with the turbulent structure of the fluid in the vicinity of the wall has been proposed. Additional study, both experimental and theoretical, is in progress to clarify these results even further and to discover how they may be applied to advantage in industrial processes.

References

1. Soo, S.L., "Fluid Dynamics of Multiphase Systems", Blaisdell Publishing Co. (1967).
2. Saffman, P.G., J. Fluid Mech., 13, 120 (1962).
3. Julian, F.M., and Dukler, A.E., A.I.Ch.E. J., 11, 853 (1965).
4. Pfeffer, R., Rossetti, S.J., and Lieblein, S., NASA TN, D3603 (1966).
5. Boothroyd, R.G., Trans. Instn. Chem. Engrs., 44, 306 (1966).
6. Vogt, E.G. and White, R.R., Ind. Eng. Chem. 40, 1731 (1948).
7. Belden, D.H. and Kassel, L.S., Ind. Eng. Chem., 41, 1174 (1949).
8. Wen, C.Y. and Simons, H.P., A.I.Ch.E. J., 5, 263 (1959).
9. Dogin, M.E. and Lebedev, V.P., Int. Chem. Eng., 2, 64 (1962).
10. Doig, I.A. and Roper, G.H., I & EC Fund., 6, 247 (1967).
11. Mitlin, L., "A Study of Pneumatic Conveying with Special Reference to Particle Velocity and Pressure Drop During Transport", Ph.D. Thesis, Univ. of London (1954).

12. Farber, L., Ind. Eng. Chem., 41, 1184 (1949).
13. Mehta, N.C., Smith, J.M., and Comings, E.W., Ind. Eng. Chem., 49, 986 (1957).
14. Schluderberg, D.C., Whitelaw, R.L. and Carlson, R.W., Nucleonics, 19, 67 (1961).
15. Peskin, R.L., Quarterly Reports 63-1 and 64-1, Contract No. AT (30-1) 2930, Rutgers Univ. (1963).
16. McCarthy, H.E. and Olson, J.H., I & EC Fund., 7, 471 (1968).
17. Tien, C.L., and Quan, V., Paper No. 62-HJ-15 ASME (1962).
18. Sproull, W.T. Nature, 190, 976 (1961).
19. Soo, S.L. and Trezek, G.J., I & EC Fund., 5, 388 (1966).
20. Fabula, A.G., Proc. Fourth Intern. Congr. on Rheology, 455 (1965).
21. Ernst, W.D., A.I.Ch.E. J., 12, 581 (1966).
22. Hershey, H.C. and Zakin, J.L., I & EC Fund., 6, 381 (1967).
23. Astarita, G., I & EC Fund., 4, 354 (1965).
24. Daily, J.W. and Bugliarello, G., Tappi, 44, 497 (1961).
25. Bobkowicz, A.J. and Gauvin, W.H., Can. J. Chem. Eng., 43, 87 (1965).
26. Rossetti, S.J., "Pressure Drop and Flow Characteristics of Dilute Gas-Solid Suspensions", Ph.D. Thesis, City Univ. of N.Y. (1969).
27. Foust, A.S., Wenzel, L.A., Clump, C.W., Maus, L., and Andersen, L.B., "Principles of Unit Operations", John Wiley and Sons, Inc. (1960).
28. Orr, C., "Particulate Technology", The MacMillan Company (1966).
29. Owen, P.R., J. Fluid Mech. 39, part 2, 407-432 (1969).
30. Paterson, G.K., "Turbulence Measurements in Polymer Solutions Using Hot-Film Anemometry", Ph.D. Thesis, University of Missouri at Rolla (1966).

Nomenclature

A	cross sectional area of tube, ft.^{2}
a,b	constants in equation (7)
D	tube diameter, ft.
D_p	particle diameter, microns or ft.
f	Blasius friction factor, dimensionless
g_c	gravitational constant, lbs mass-ft./lbs force-sec^2
F	force exerted on target, lbs force
K_1, K_2	constants in equation (2)
K_1^1,K_2^1	constants in equation (6)
I	intensity of turbulence, dimensionless
L	length of test section, ft.
m_g,m_p,m_s	mass of gas, particles, suspension, lbs.
ΔP	pressure drop across test section, lbs force/ft.^{2}
ΔP_m	measured pressure drop, lbs force/ft.^{2}
Re	gas Reynolds number, dimensionless
t	time, sec
t_e	eddy characteristic time, sec
t_l	large eddy characteristic time, sec
t_R	relaxation time, sec
u_τ	friction velocity, ft/sec
$\bar{v}$	average velocity of gas, ft/sec
v_c	centerline gas velocity
v_s	velocity of suspension, ft/sec

Nomenclature (cont.)

V_{ST}	strain gage output, millivolts
W_p	particle flow rate, g/sec
ρ_g	gas density, lbs/ft.^{3}
ρ_p	particle density, lb/ft^3
μ	gas viscosity, lbs/ft-sec
μ	refers to particle diameter, microns
η	loading ratio, particle mass flow rate/gas mass flow rate, dimensionless

Subscripts

g	gas
p	particles
s	suspension

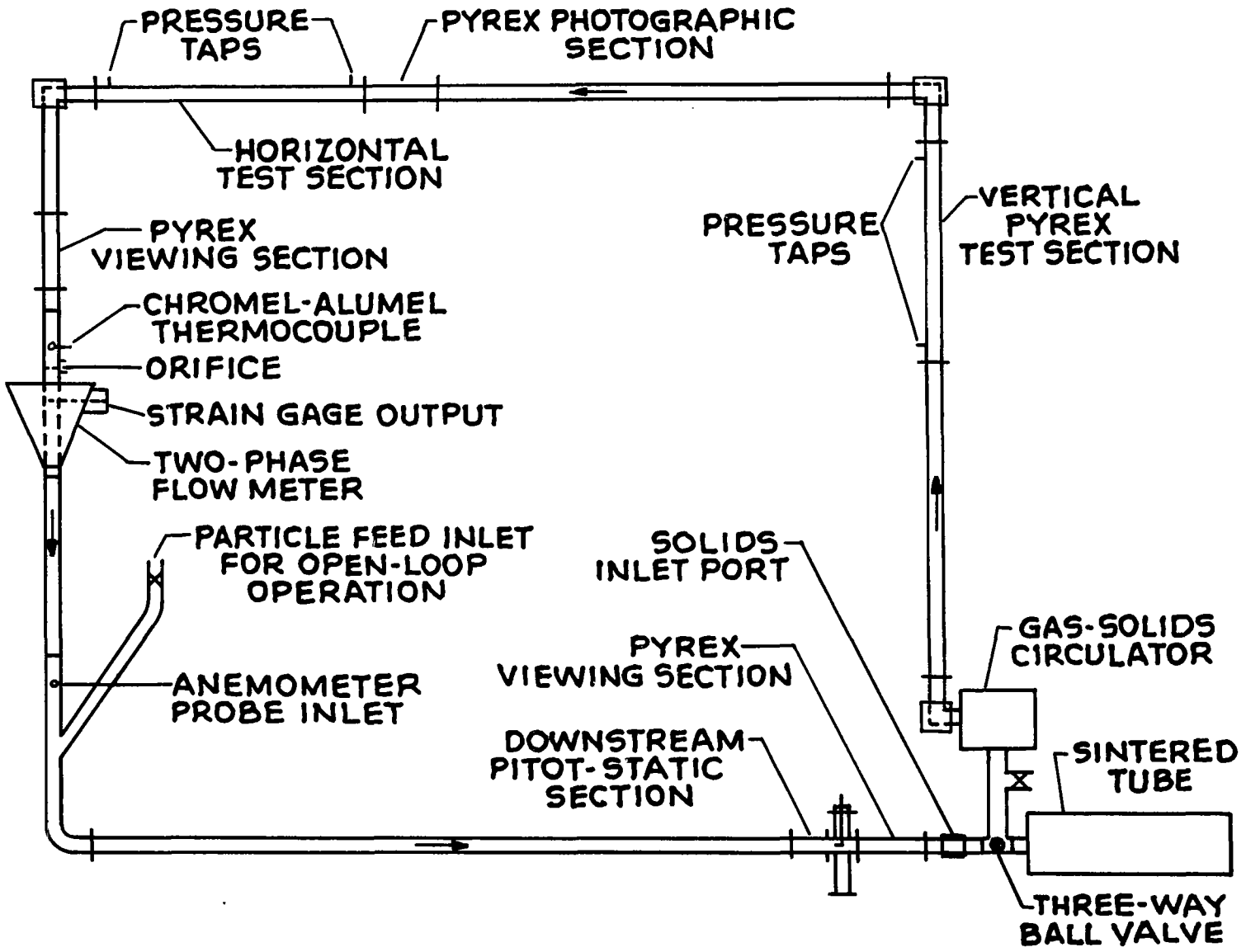

Figure 1. - Schematic diagram of closed loop.

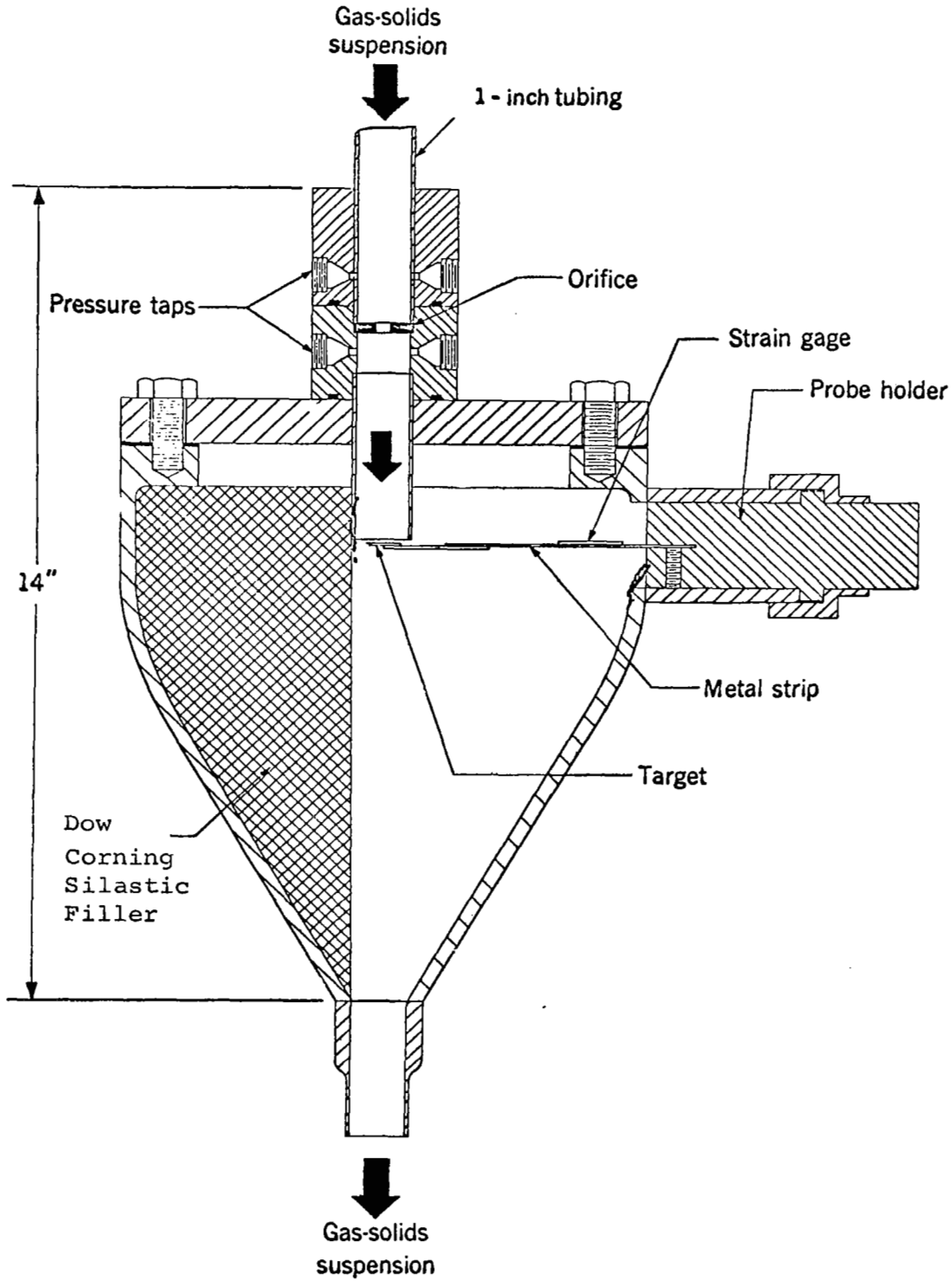

Figure 2. - Two phase mass flowmeter.

(a) Before recirculation – 700x magnification

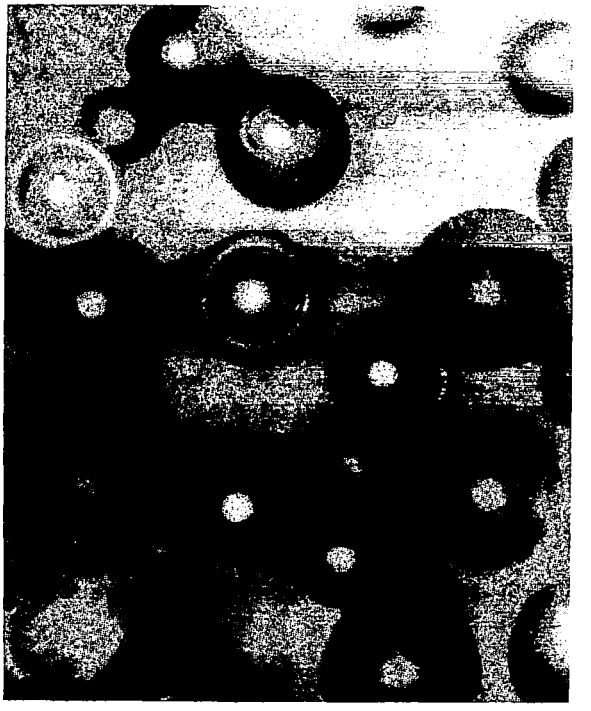

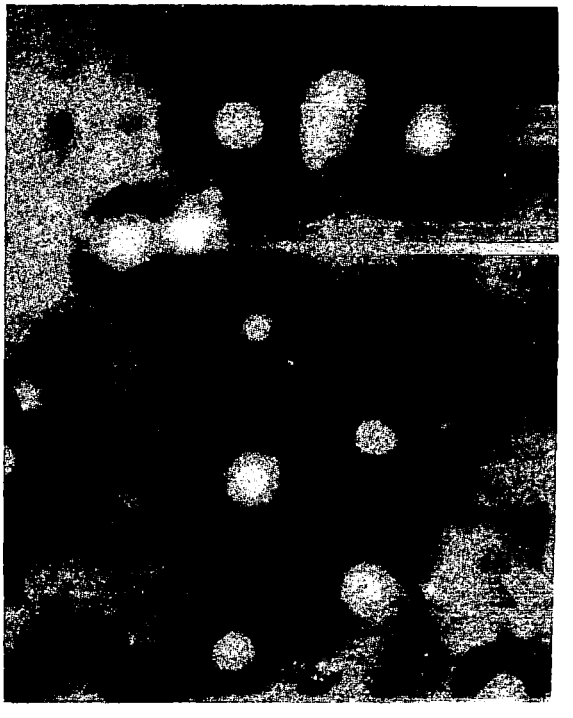

(b) After recirculation for 3480 seconds in the closed loop – 700x magnification.

Figure 3. - Microphotographs of 30μ glass beads.

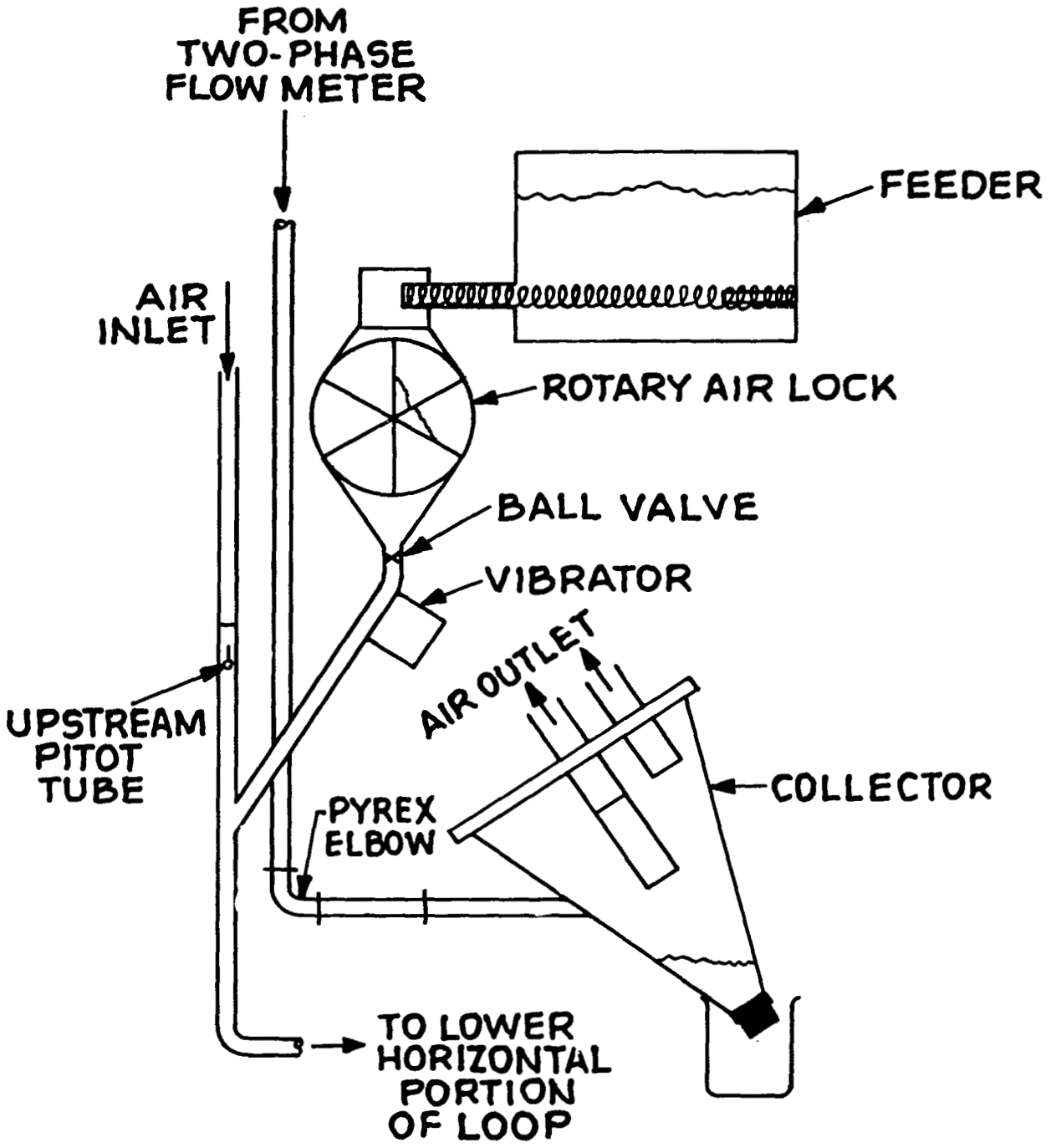

Figure 4. - Schematic diagram of open loop.

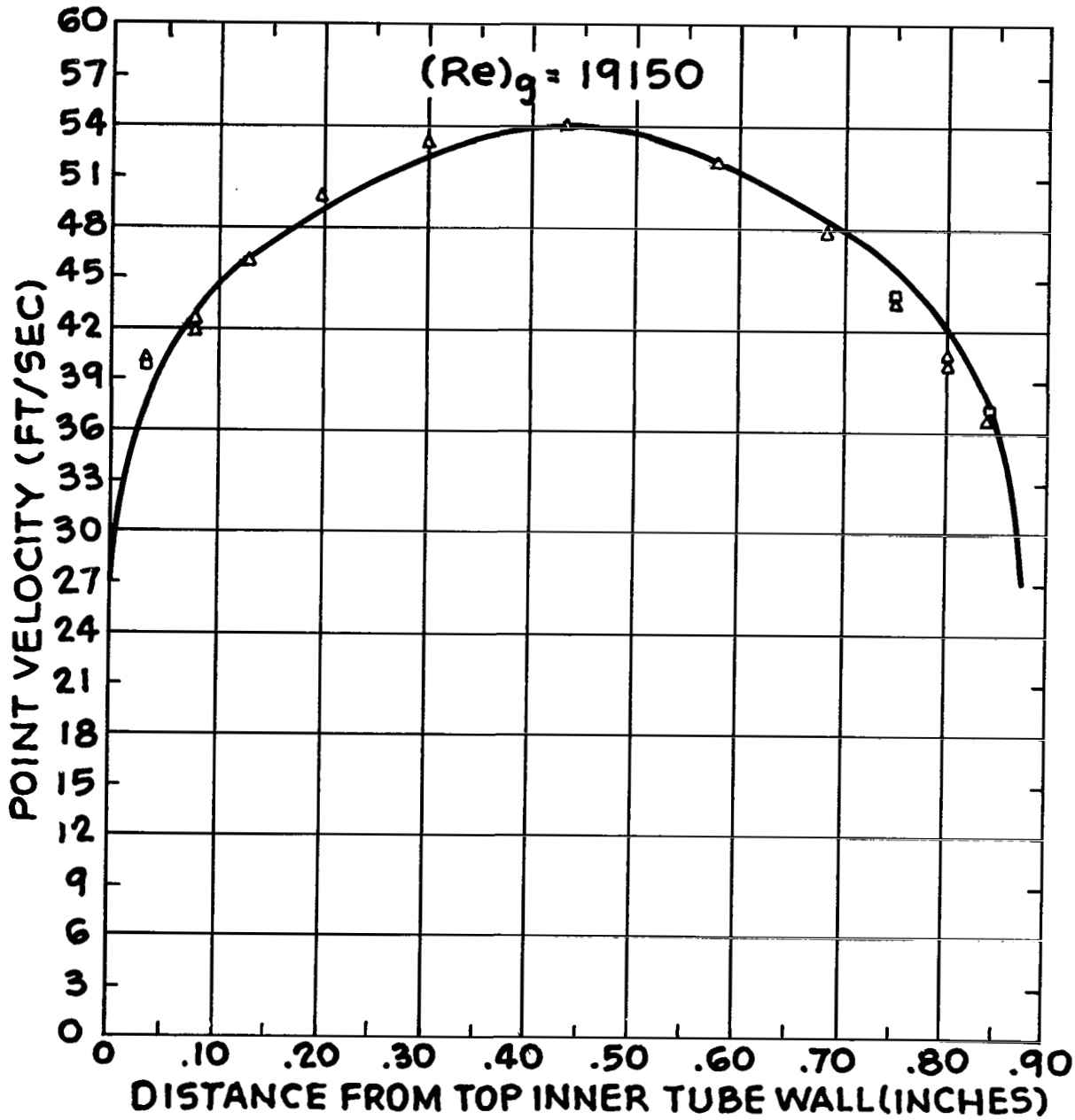

Figure 5. - Typical gas velocity profile.

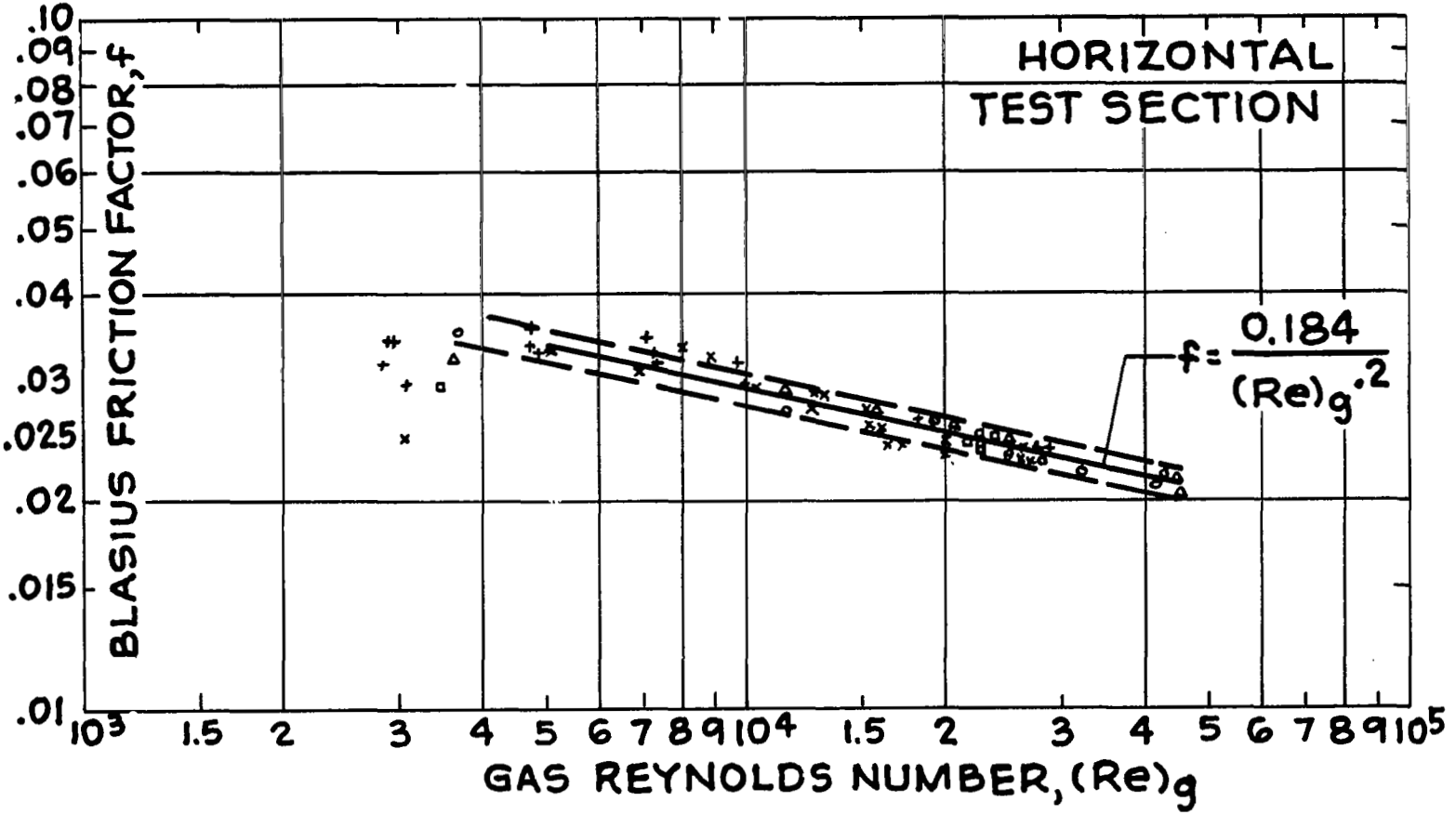

Figure 6. - Gas friction factor as function of gas Reynolds number for horizontal test section.

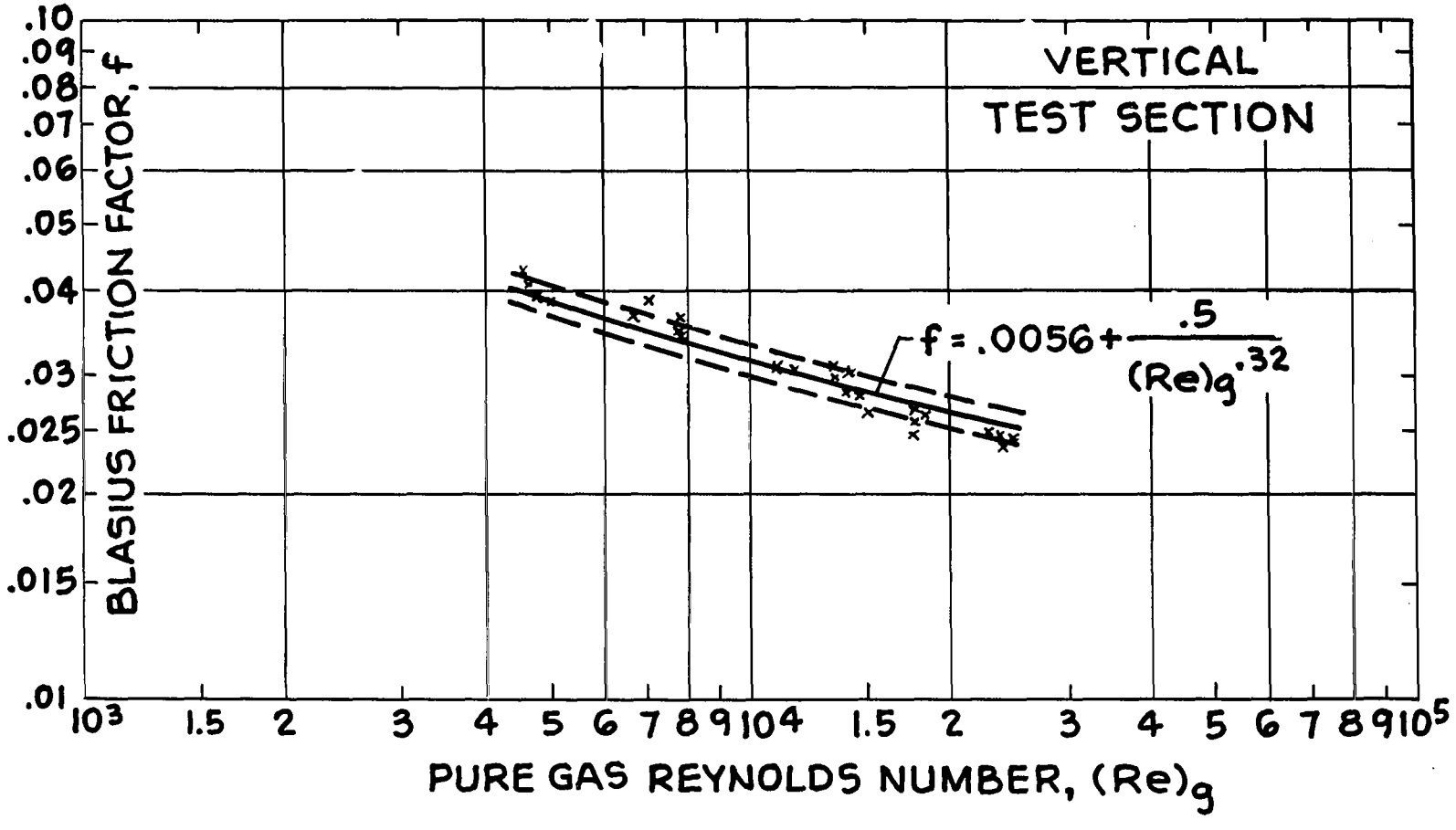

Figure 7. - Gas friction factor as function of gas Reynolds number for vertical test section.

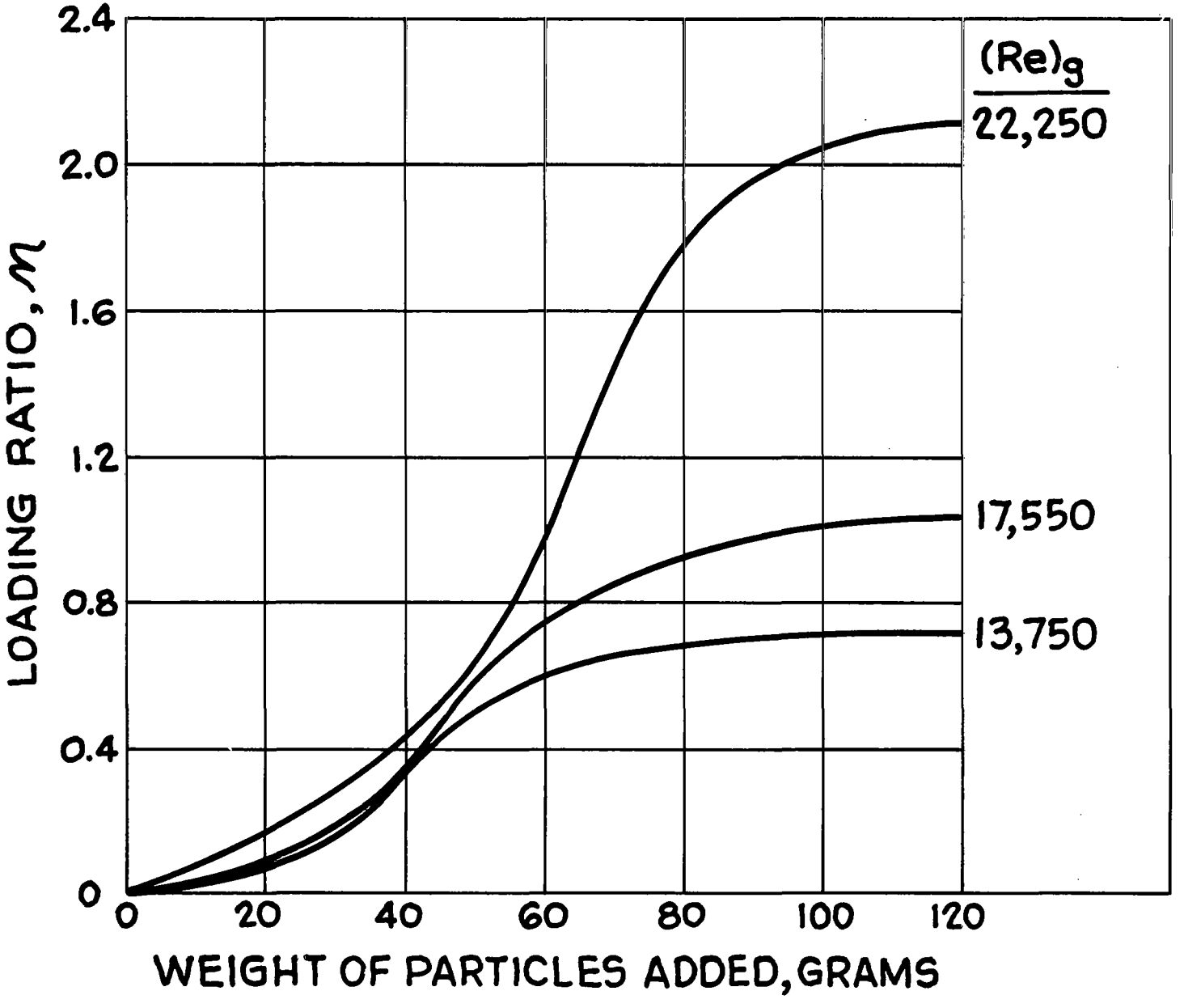

Figure 8. - Loading ratio as function of weight of 30μ particles added to closed loop.

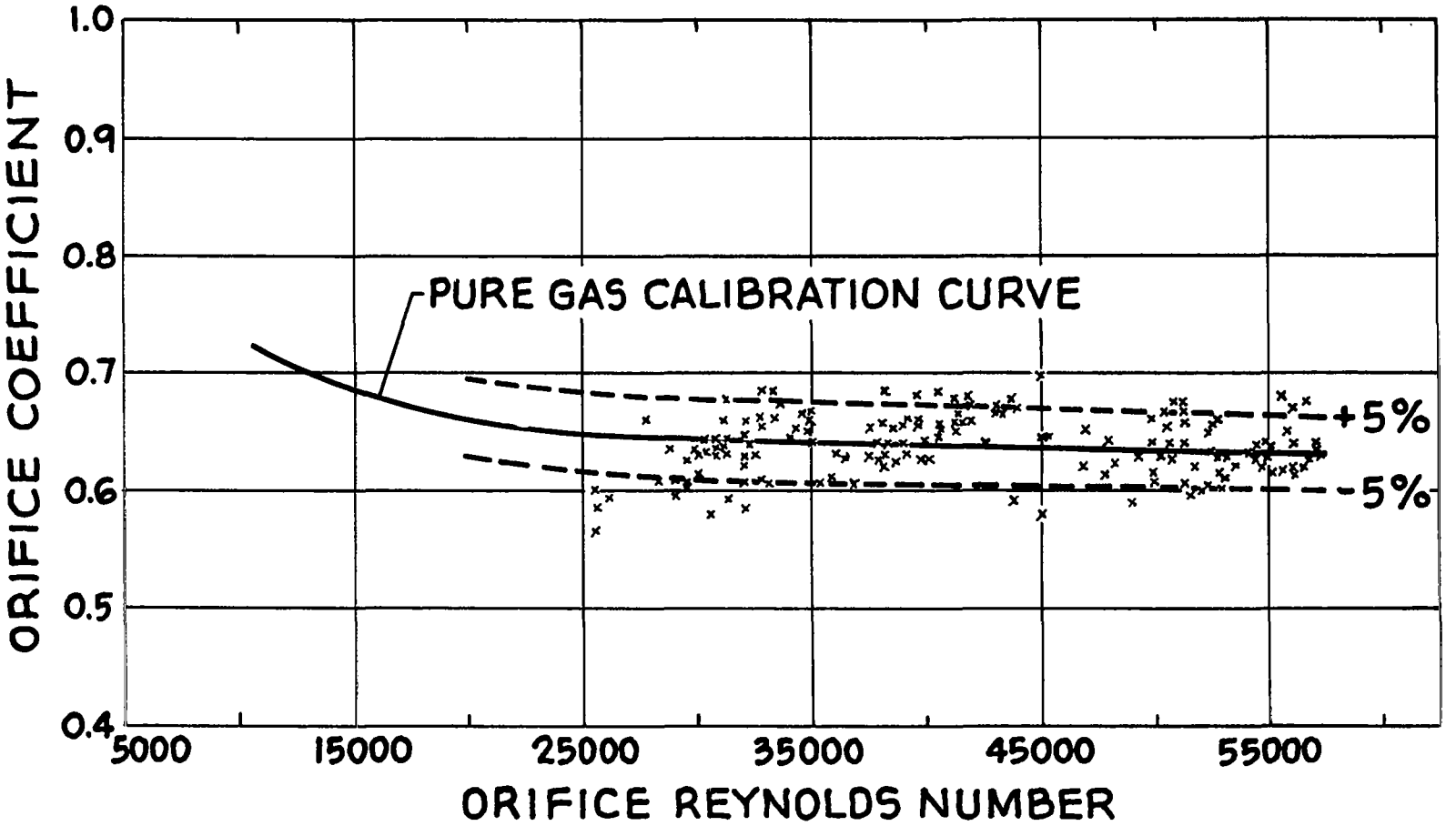

Figure 9. - Orifice coefficient as function of orifice Reynolds number for all particle sizes and loading ratios.

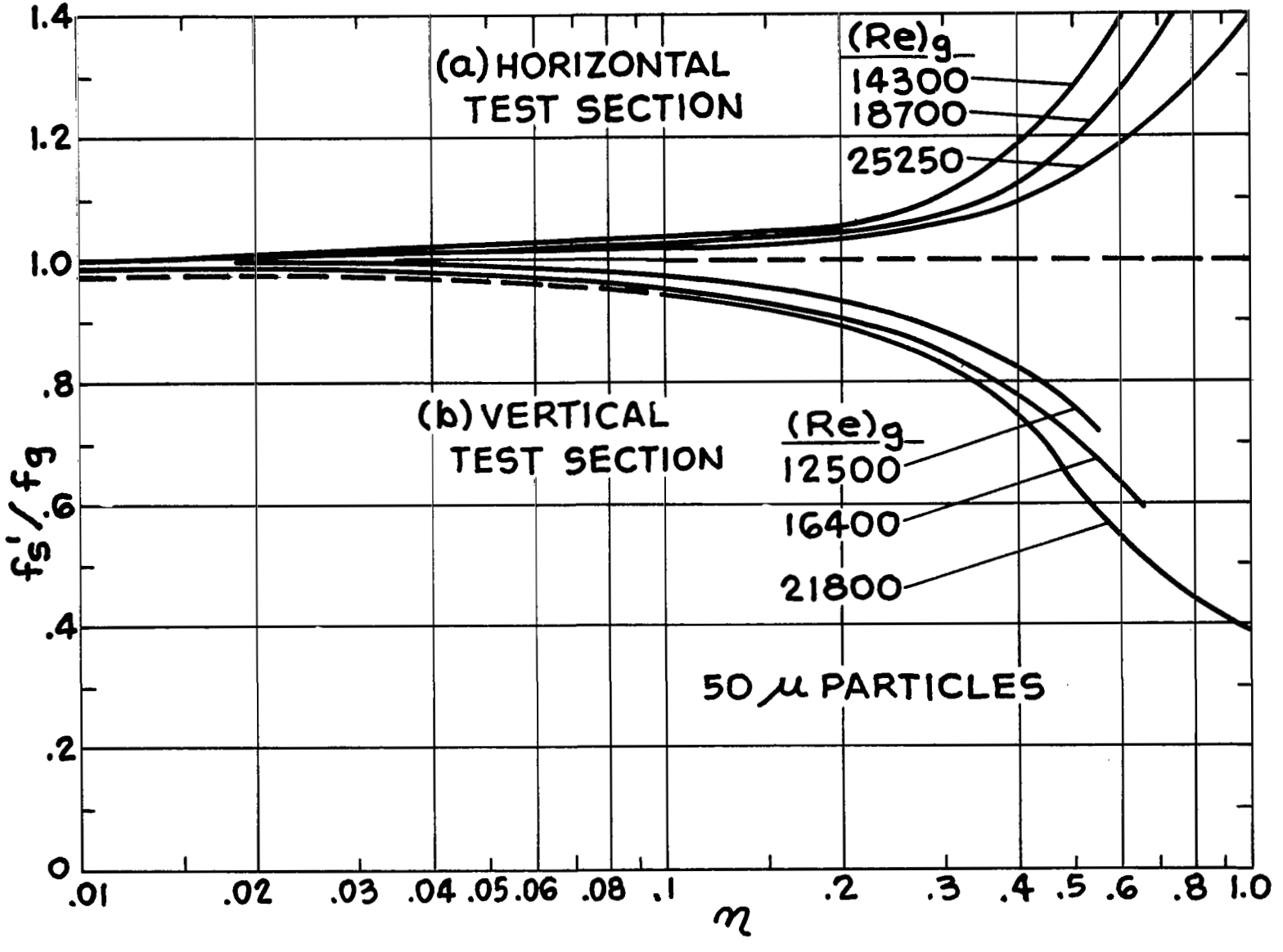

Figure 10. - Friction factor ratio as function of loading ratio with Reynolds number as parameter for 50μ particles.

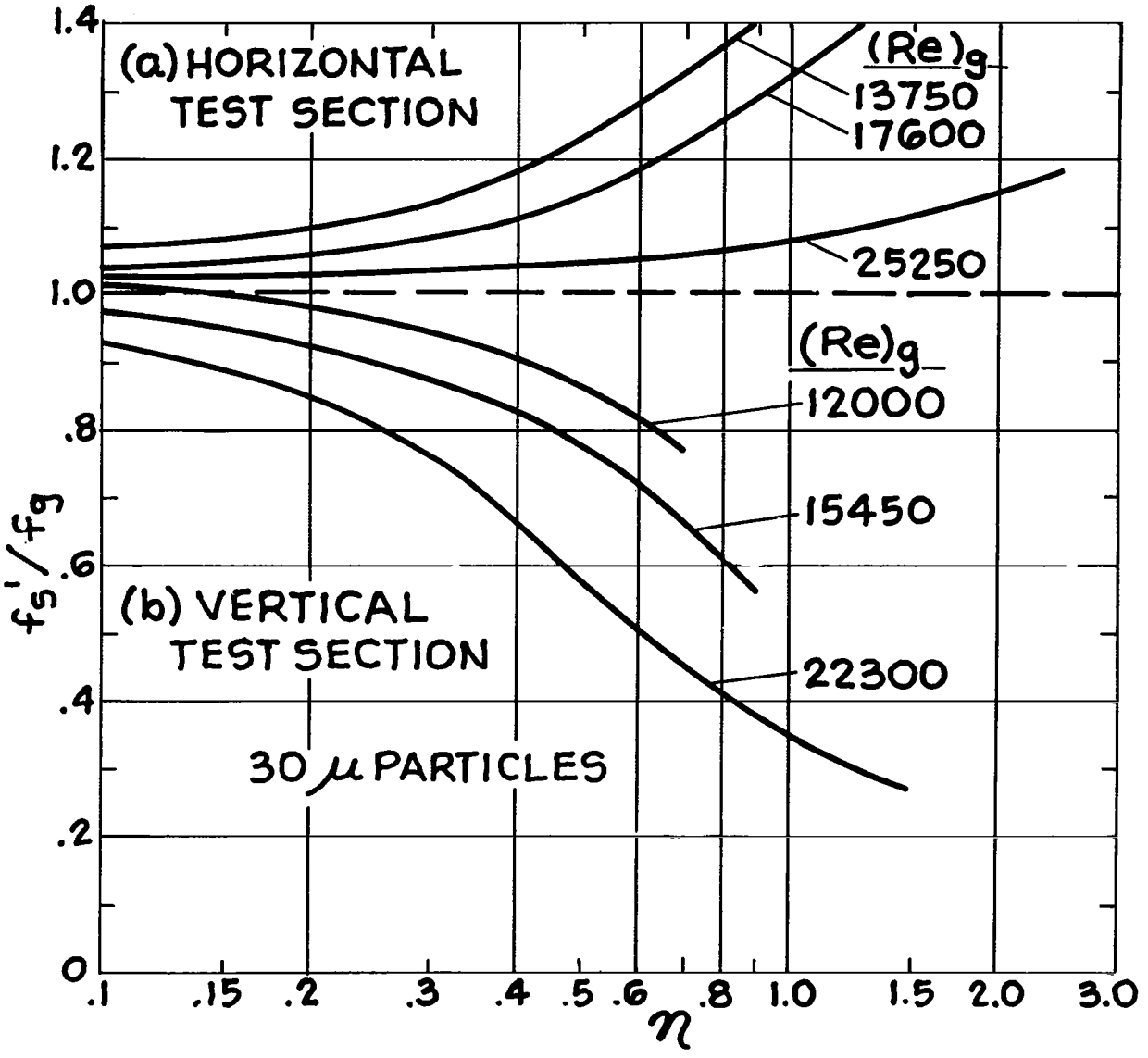

Figure 11. - Friction factor ratio as function of loading ratio with Reynolds number as parameter for 30μ particles.

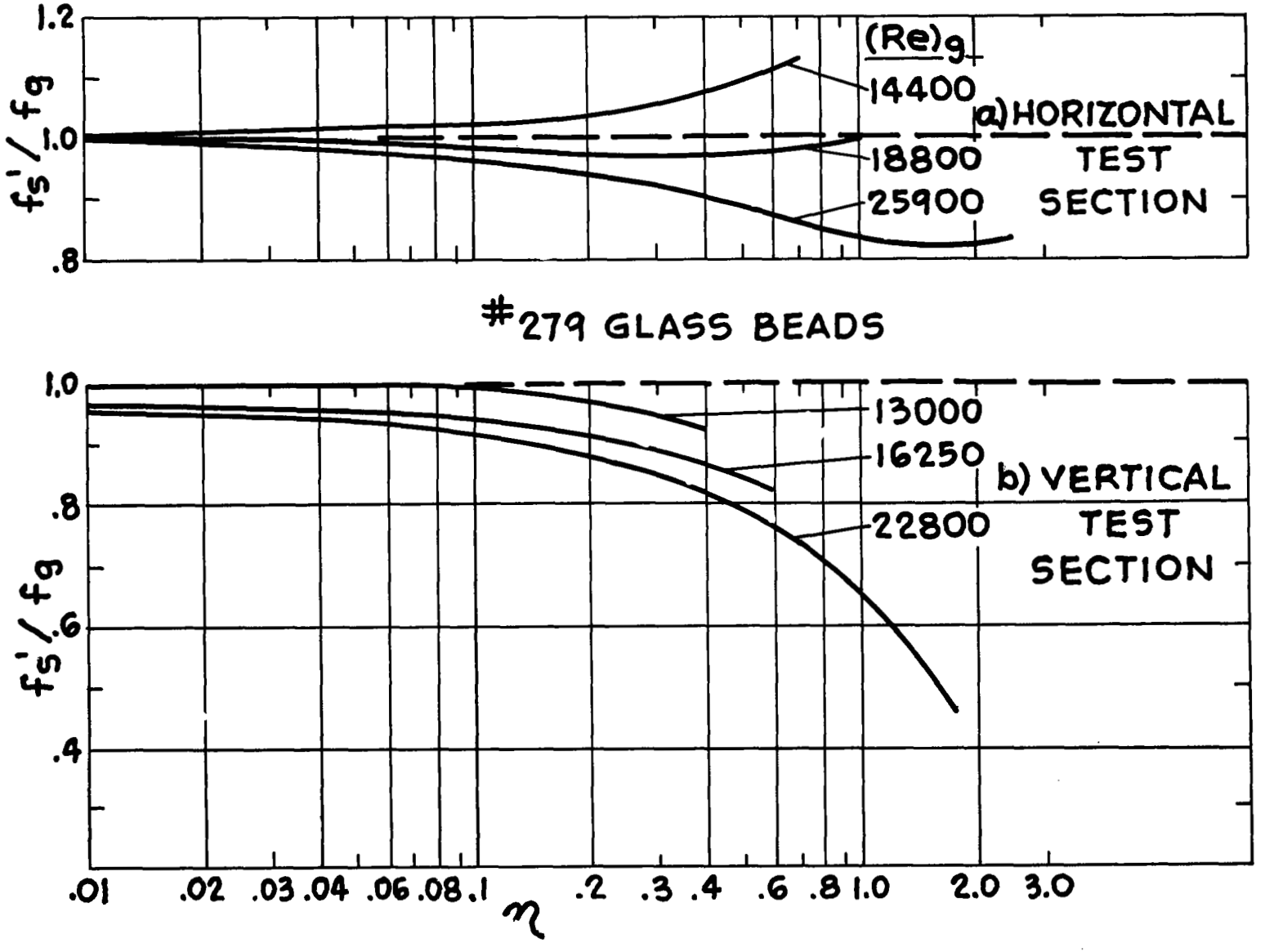

Figure 12. - Friction factor ratio as function of loading ratio with Reynolds number as parameter for no. 279 glass beads.

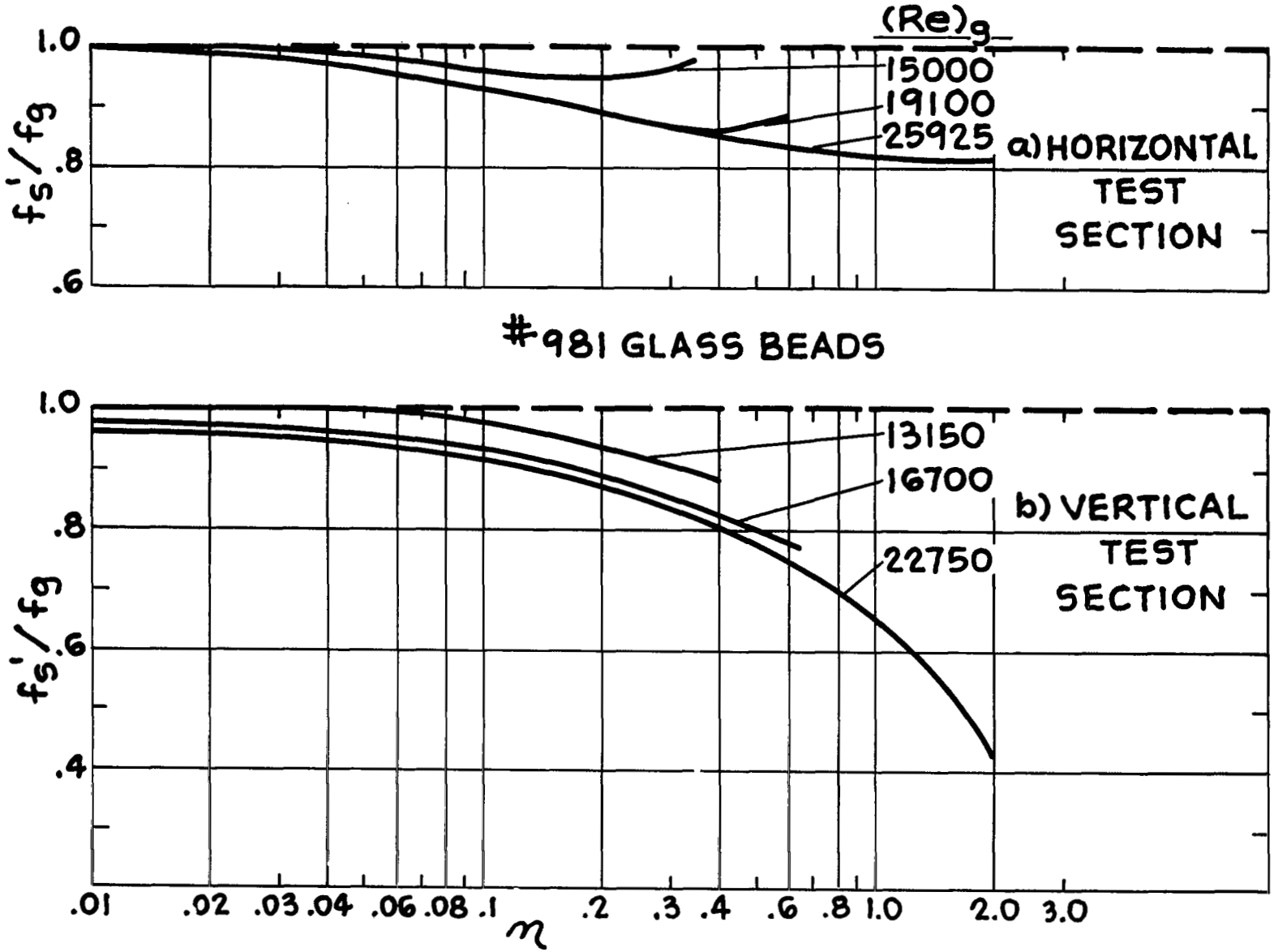

Figure 13. - Friction factor ratio as function of loading ratio with Reynolds number as parameter for no. 981 glass beads.

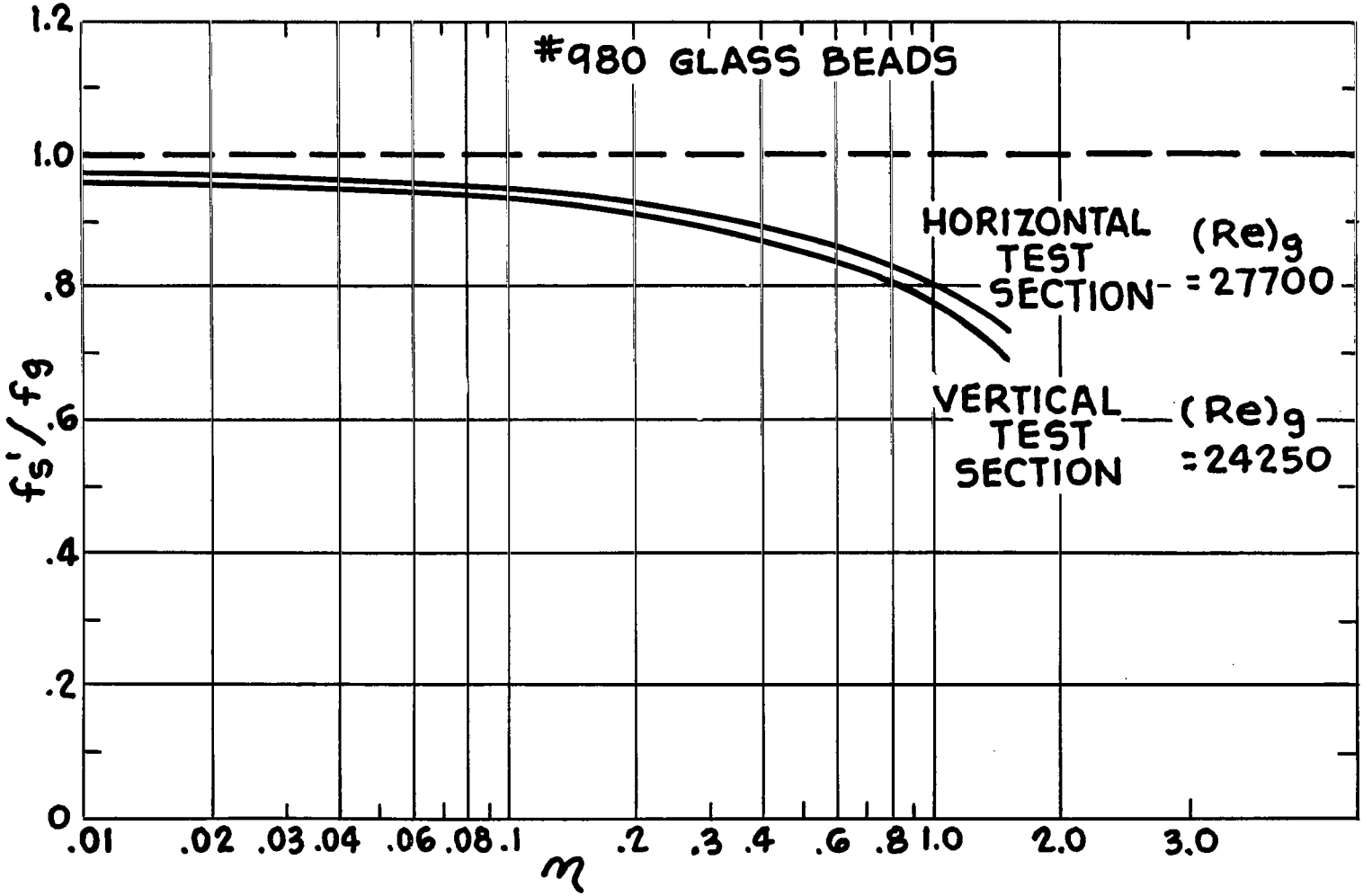

Figure 14. - Friction factor ratio as function of loading ratio with Reynolds number as parameter for no. 980 glass beads.

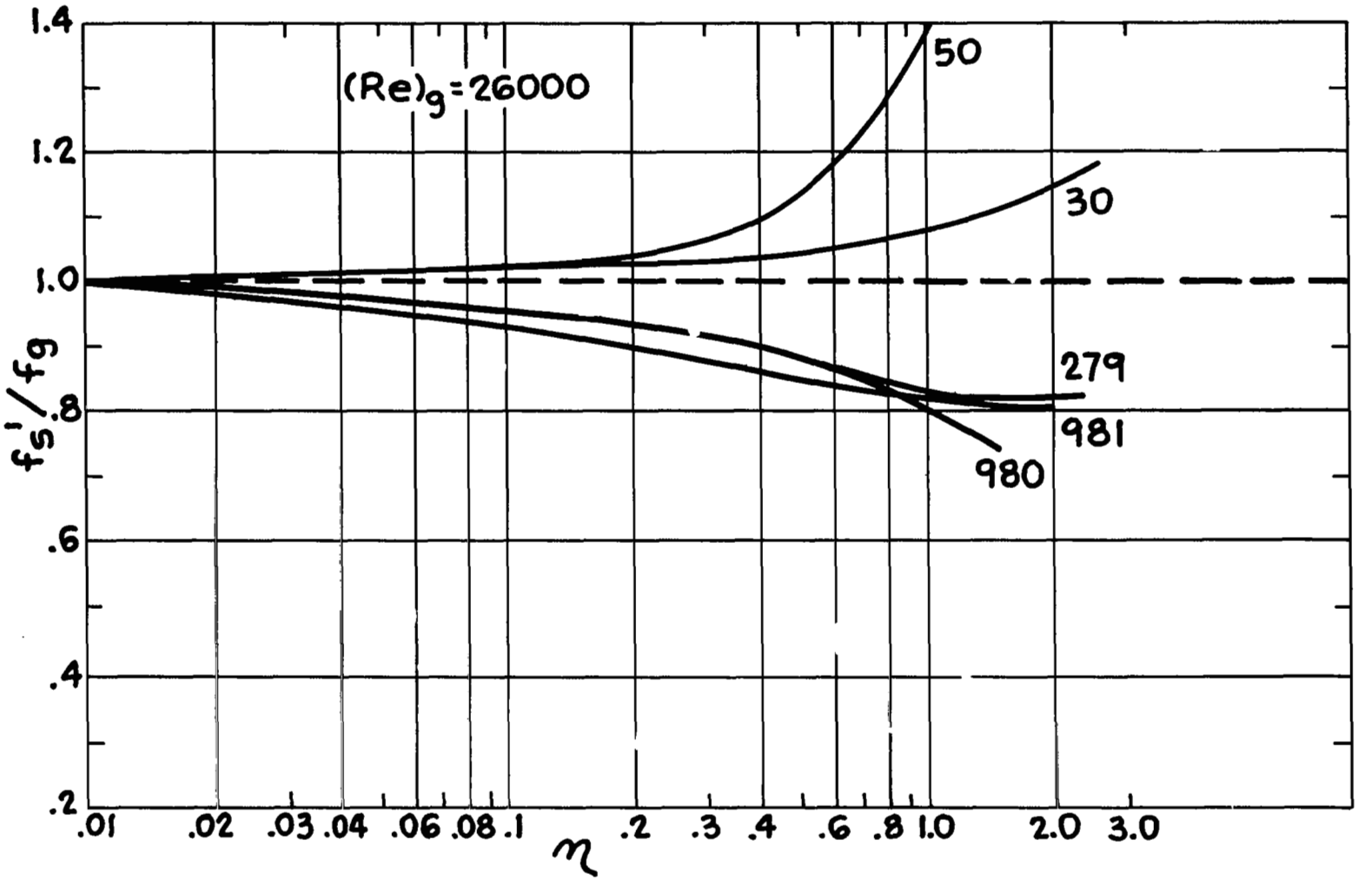

Figure 15. - Friction factor ratio as function of loading ratio in horizontal test section.

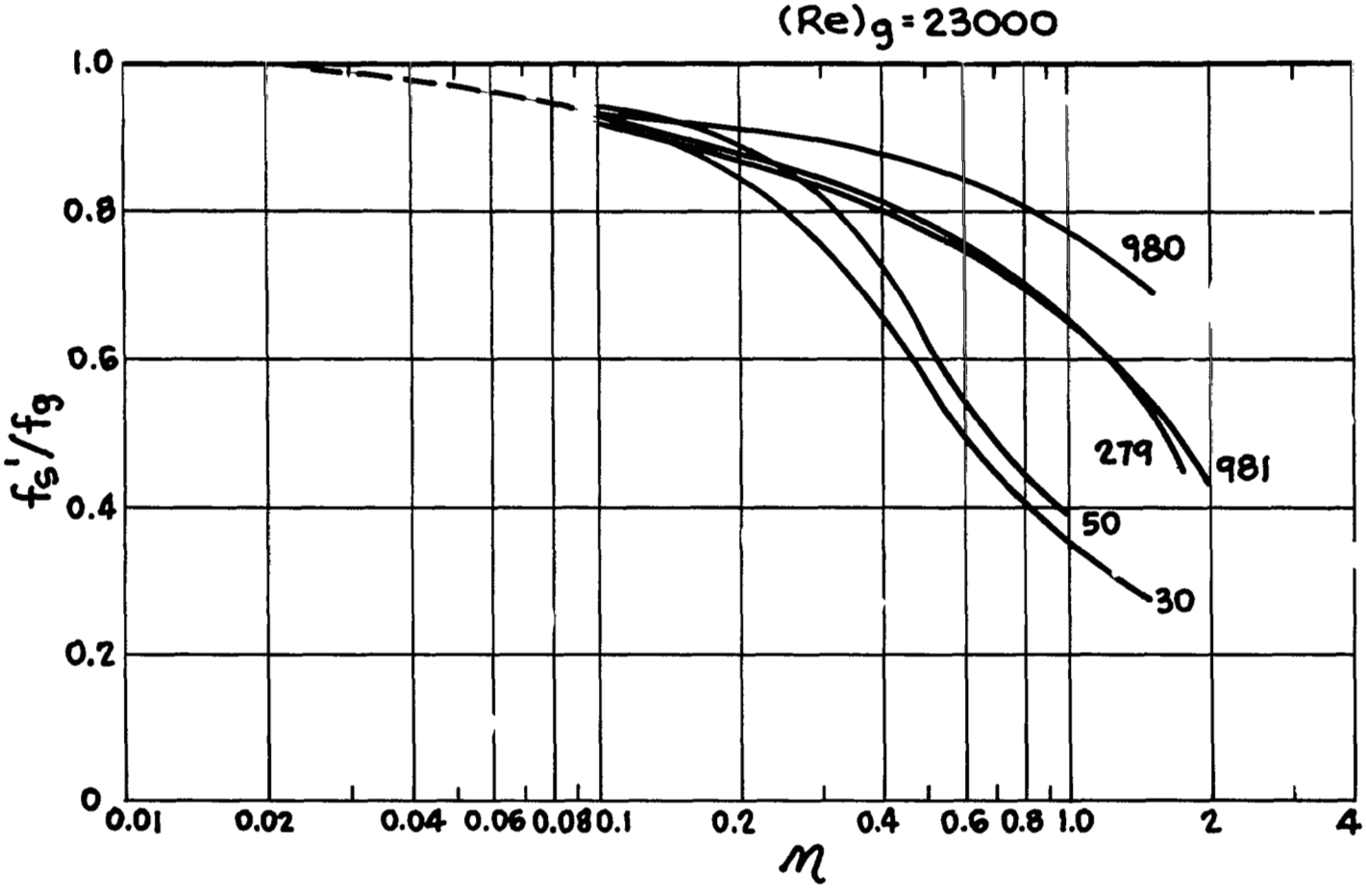

Figure 16. - Friction factor ratio as function of loading ratio in vertical test section.

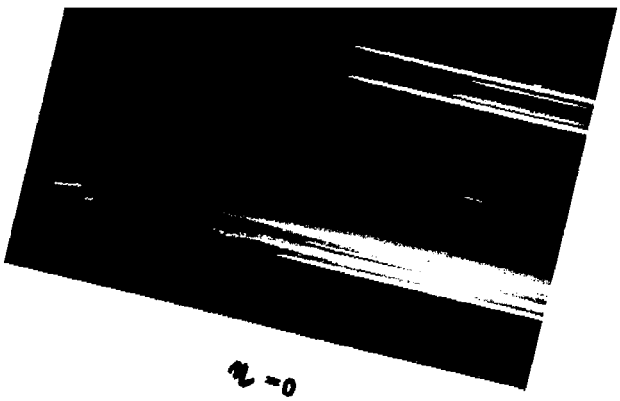

$\eta = 0$

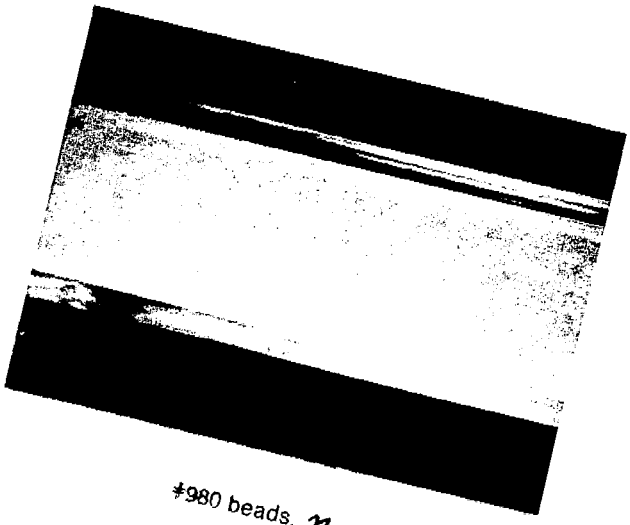

#980 beads, $\eta = .20$

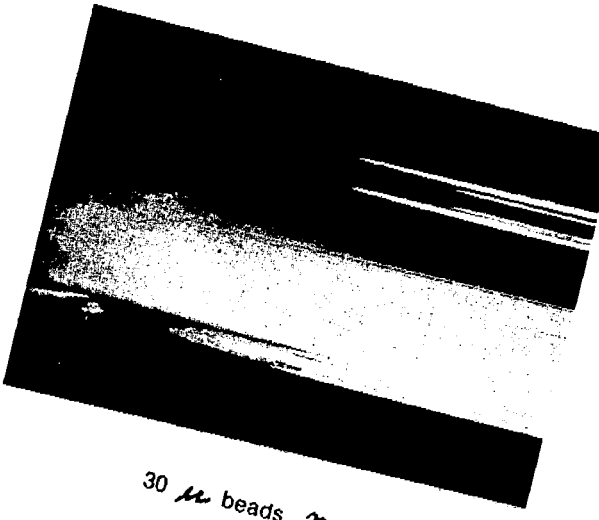

30 μ beads, $\eta = .50$

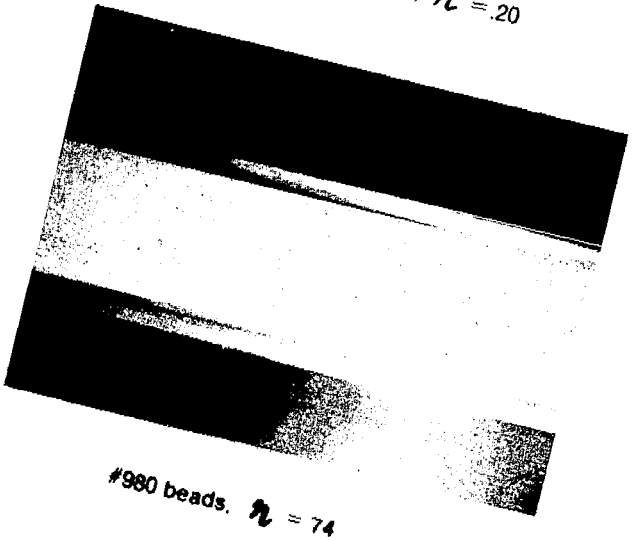

#980 beads, $\eta = 74$

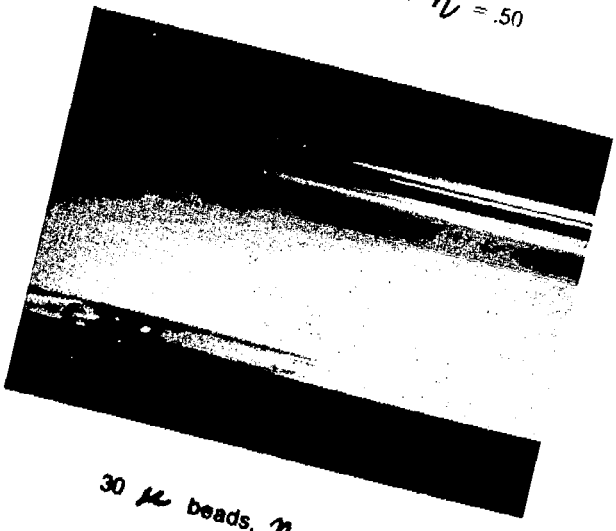

30 μ beads, $\eta = 1.44$

Figure 17. - Gross flow photographs.

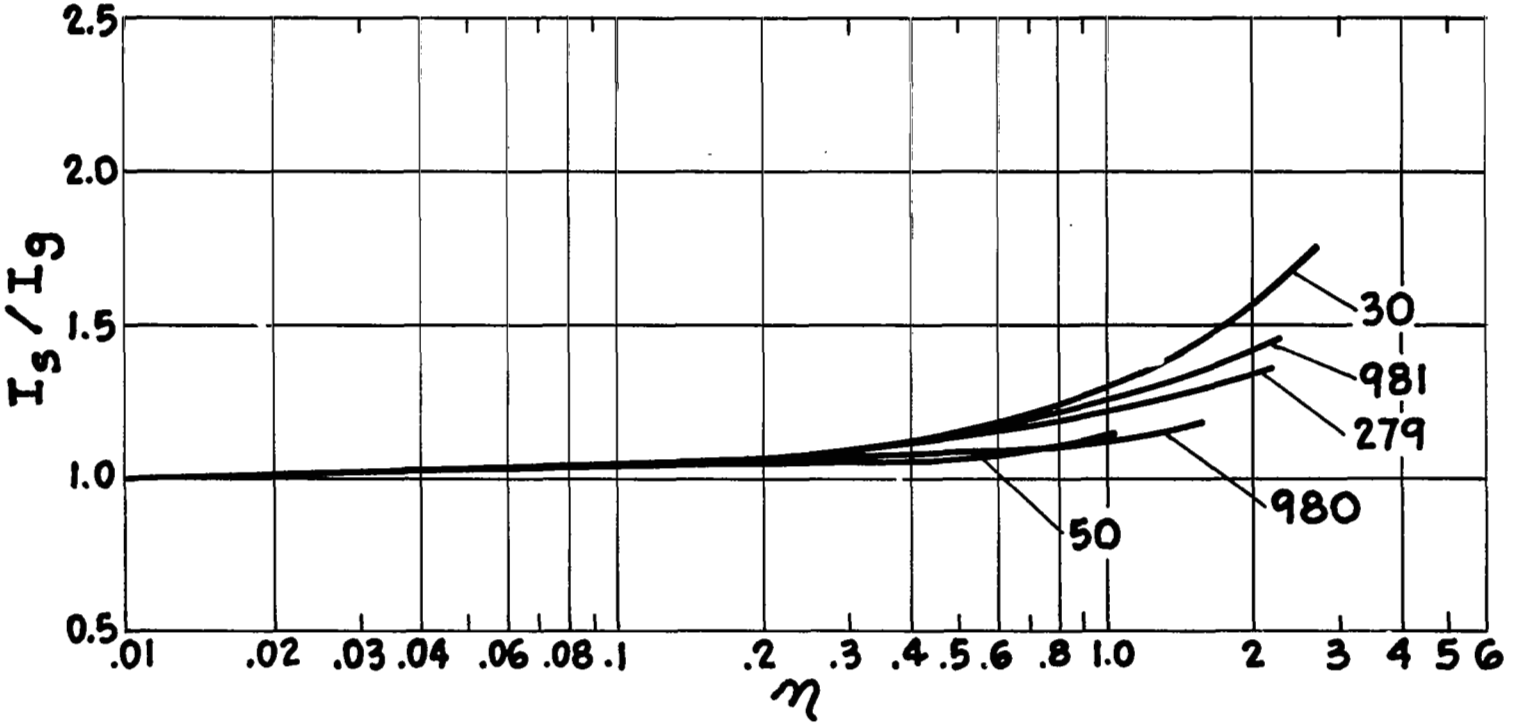

Figure 18. - Relative turbulence intensity ratio as function of loading ratio.